Supporting Information

Orange/Cyan Emissive Sensors of Sb^{3+} for Probing Water via Reversible Phase Transformation in Rare-Earth-Based Perovskite Crystals

Yexin Huang,[a] Yuexiao Pan,[a]* Chengdong Peng,[a] Yihong Ding,[a] Hongzhou Lian,[b] Liyi Li,[c]* and Jun Lin [b]*

[a]*Key Laboratory of Carbon Materials of Zhejiang Province, College of Chemistry and Materials Engineering, Wenzhou University, Wenzhou 325035, P. R. China.*

[b]*State Key Laboratory of Rare Earth Resource Utilization, Changchun Institute of Applied Chemistry, Chinese Academy of Sciences, Changchun 130022, P. R. China.*

[c]*Innovative Drug and Imaging Agent R&D Center, Research Institute of Qsinghua, Pearl River Delta, Guangzhou, P. R. China.*

2. Experimental

2.5. Characterization

The single-crystal X-ray diffraction data were collected using a SMART APE II DUO X-ray four-circle single-crystal diffractometer (Bruker) equipped with a CCD-detector, a graphite monochromator, and a Cu K radiation source. The powder X-ray diffraction (PXRD) patterns of the crystals were collected on a Bruker (Karlsruhe, Germany) D8 Advance XRD with graphite monochromatized Cu Kα radiation (λ = 0.15418 nm) in the two degrees range from 10-80°. High-resolution transmission electron microscopy (HRTEM) observation was performed by using a JEOL 2100F high-resolution transmission electron microscope using an accelerating voltage of 200 kV with an attached energy-dispersive x-ray energy dispersive spectrum spectrometer (EDS). The chemical composition on the surface of the particles was analyzed by using x-ray photoelectron spectra (XPS) conducted on a ESCALAB 250Xi versa

probe spectrometer (analyzer resolution ≤ 0.5 eV) with a monochromatic of Al Kα radiation ($h\nu$ = 486.6 eV). The photoluminescence (PL) excitation and PL emission spectra were recorded on a FluoroMAX-4-TCSPC fluorescence spectrophotometer (Horiba Jobin Yvon Inc). The PL decay curves were recorded on an FLS980 spectrometer (Edinburgh).

2.6. Computational Methodology

The first-principles density functional theory (DFT) computation was implemented by Vienna Ab initio Simulation Package (VASP).[1] Generalized gradient approximation (GGA) in the Perdew Burke Ernzerhof (PBE) form was employed for the exchange-correlation functional energies.[2] The cut-off energy was set at 350 eV for the plane wave basis set. For undoped samples, a 2 × 2 × 2 G-centered mesh was selected for Brillouin-zone K-point sampling in the unit cell. For Sb^{3+}-doped samples, a 1 × 1 × 1 G-centered mesh was used in the supercell (i.e., 2 × 2 × 1 primitive cells). The energy of the system and forces on each atom were converged to 10−5 eV and 0.003 eV/ Å.

1 G. Kresse and J. Furthmüller, Efficient iterative schemes for ab initio total-energy calculations using a plane-wave basis set, Phys. Rev. B 1996. **54**. 11169.

2 M. Ernzerhof and G. E. Scuseria, Assessment of the Perdew-Burke-Ernzerhof exchange-correlation functional, J. Chem. Phys., 1999, **110**, 5029-5036.

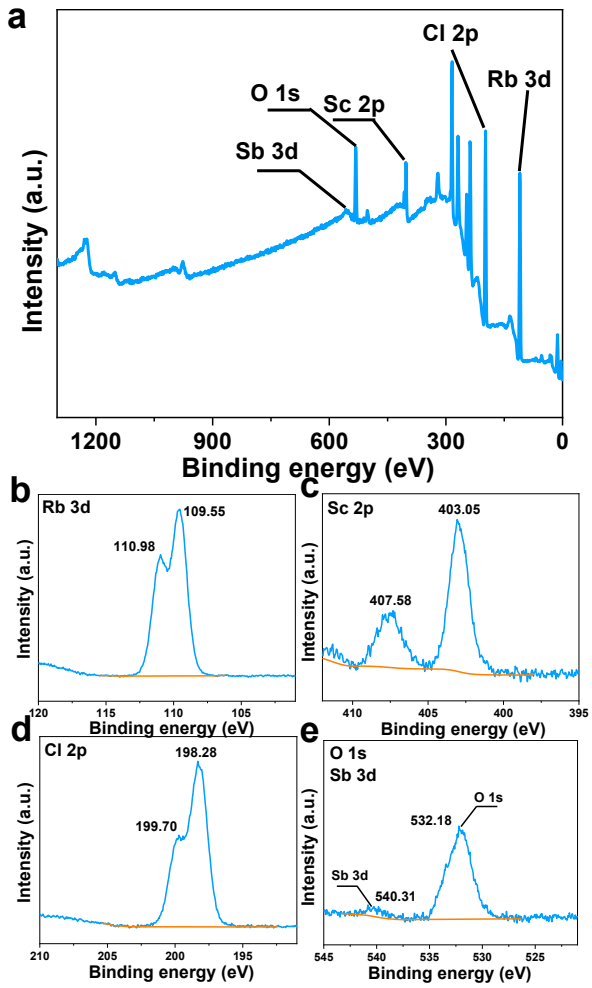

Fig. S1 (a) XPS full spectrum of $Rb_2ScCl_5 \cdot H_2O:Sb^{3+}$, (b-e) XPS spectra of the elements Rb, Sc, Cl, O, and Sb in $Rb_2ScCl_5 \cdot H_2O:Sb^{3+}$.

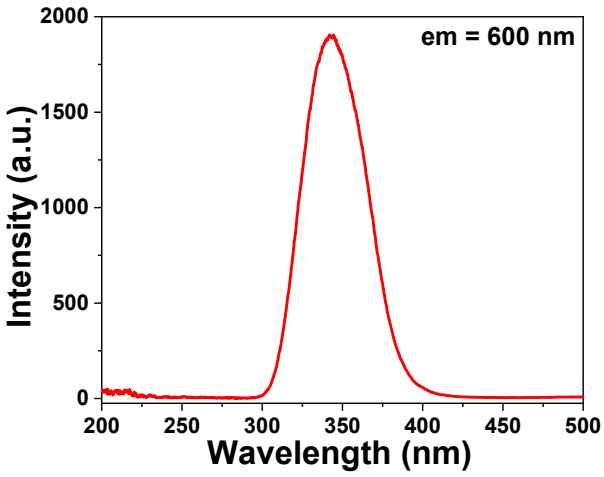

Fig. S2 Full PL excitation spectrum (λ_{em} = 600 nm) of $Rb_2ScCl_5 \cdot H_2O:Sb^{3+}$.

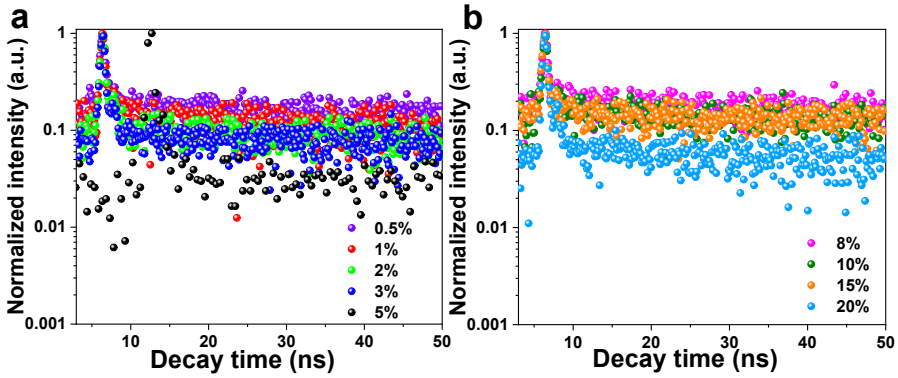

Fig. S3 (a, b) PL decay curves of $Rb_2ScCl_5{\cdot}H_2O$:x%Sb^{3+} with Sb^{3+} content increasing.

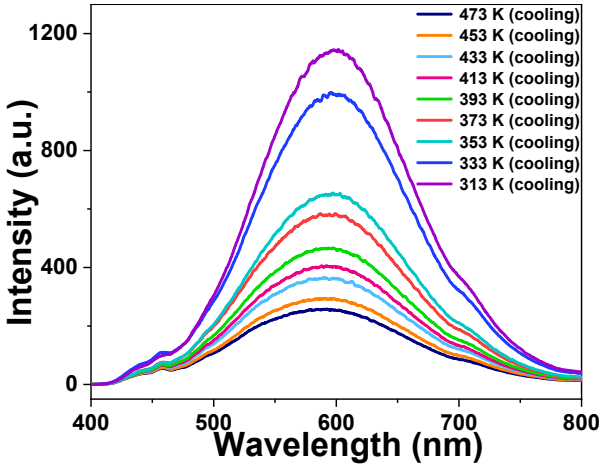

Fig. S4 Temperature-dependent PL emission spectra of $Rb_2ScCl_5{\cdot}H_2O$:Sb^{3+} during the cooling cycle.

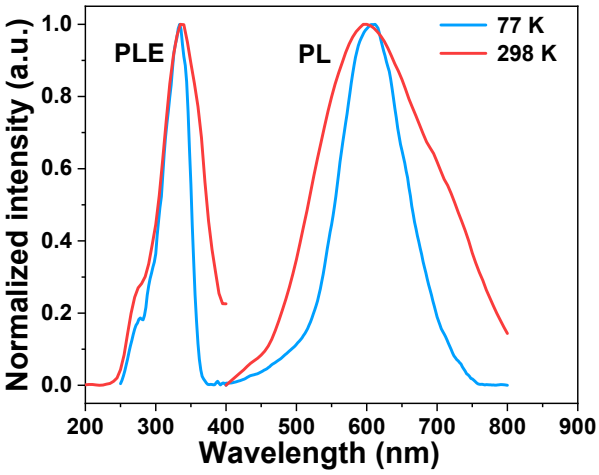

Fig. S5 Normalized PL excitation (λ_{em} = 600 nm) and emission spectra (λ_{ex} = 340 nm) of $Rb_2ScCl_5{\cdot}H_2O$:Sb^{3+} at 77 K (blue line) and 298 K (red line).

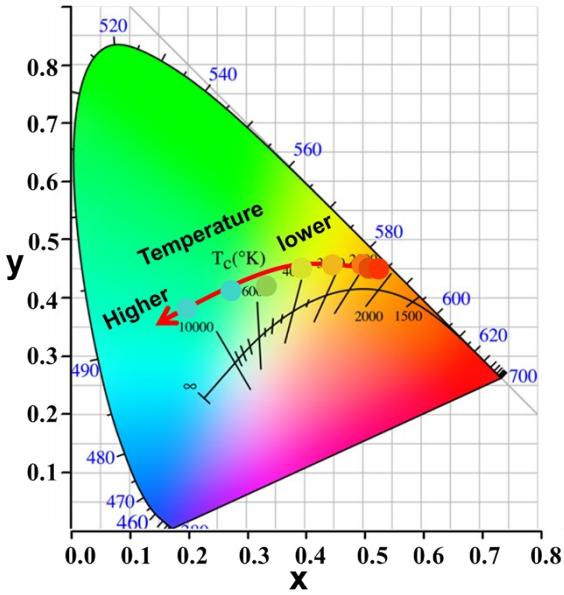

Fig. S6 CIE chromaticity coordinates of $Rb_2ScCl_5{\cdot}H_2O:Sb^{3+}$ after treatment at different temperatures.

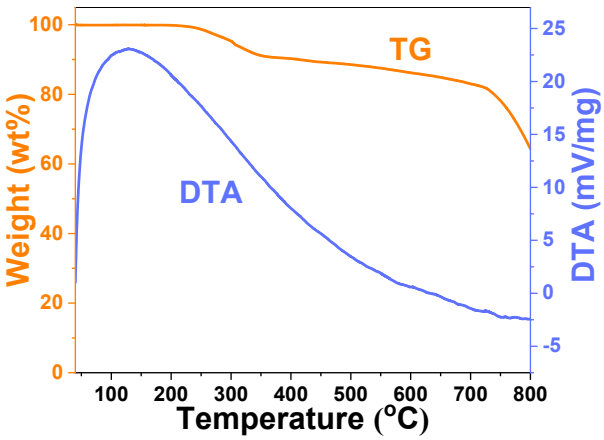

Fig. S7 Thermogravimetry/differential thermal analysis (TG-DTA) curves of $Rb_2ScCl_5{\cdot}H_2O:Sb^{3+}$ measured on Netzsch STA 449 C at a heating rate of 10 K min^{-1}.

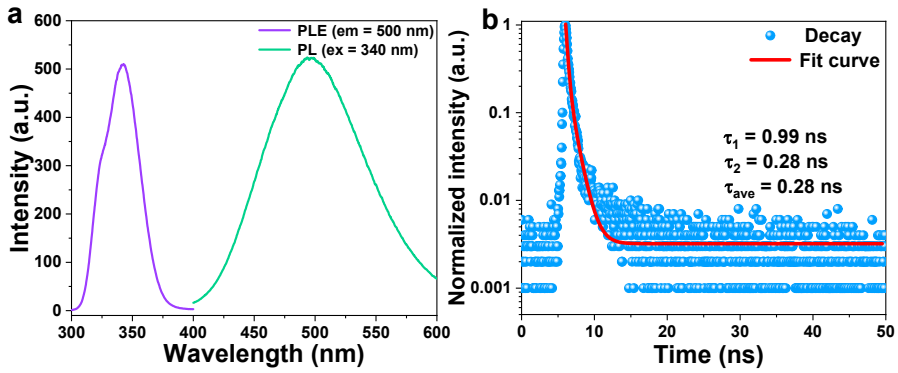

Fig. S8 (a) PL excitation (λ_{em} = 500 nm) and emission spectra (λ_{ex} = 340 nm) of $Rb_3ScCl_6:Sb^{3+}$, (b) PL decay curve of $Rb_3ScCl_6:Sb^{3+}$.

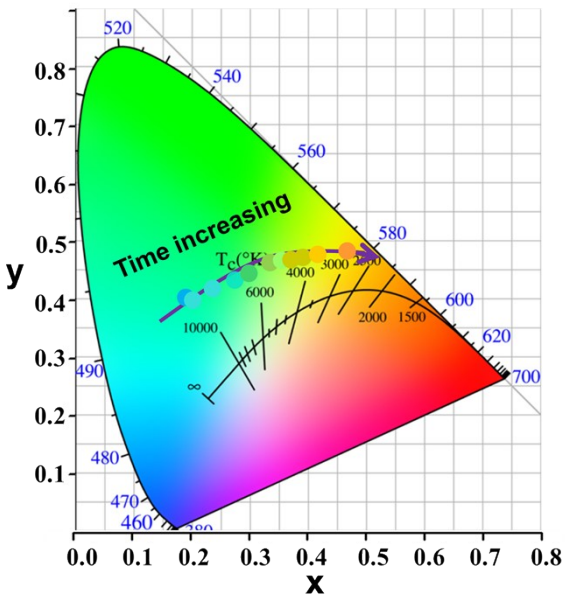

Fig. S9 CIE chromaticity coordinates of $Rb_3ScCl_6:Sb^{3+}$ with aging time between 1-60 min (finally become to be $Rb_2ScCl_5{\cdot}H_2O:Sb^{3+}$).

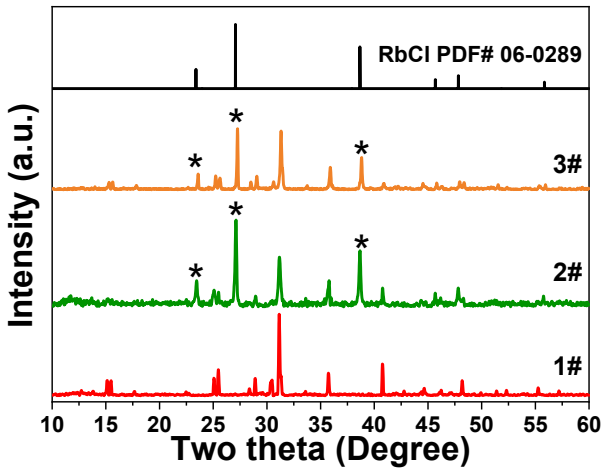

Fig. S10 XRD patterns of (1#) original $Rb_2ScCl_5{\cdot}H_2O{:}Sb^{3+}$, and the $Rb_3ScCl_6{:}Sb^{3+}$ (2#) exposed in air for 1 h and (3#) treated with 2 mL hydrochloric acid for 3 s.

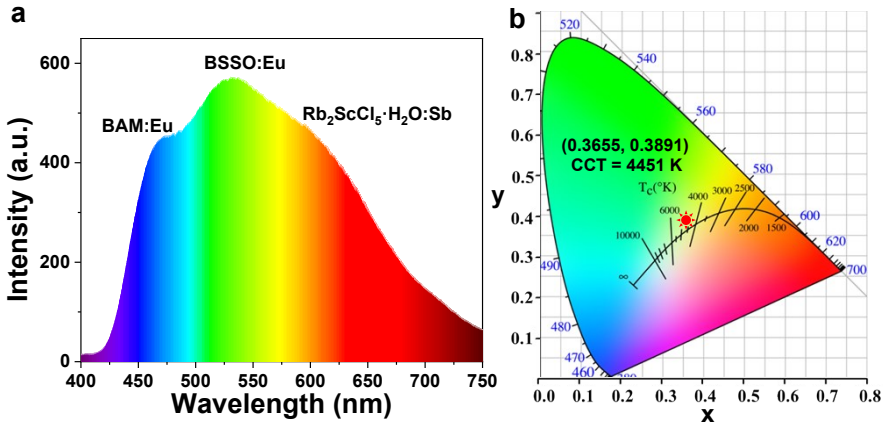

Fig. S11 (a) Electroluminescence (EL) spectrum of the WLED based on $Rb_2ScCl_5{\cdot}H_2O{:}Sb^{3+}$ at 40 mA drive current, (b) CIE color coordinates of the WLED in operation.

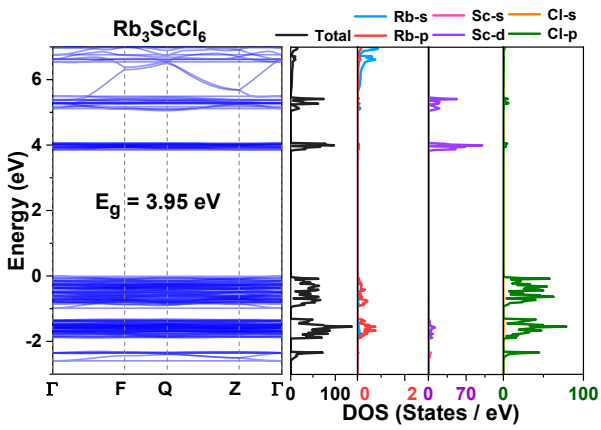

Fig. S12 Calculated electronic band structure (left) and DOS (right) of Rb_3ScCl_6 crystal.

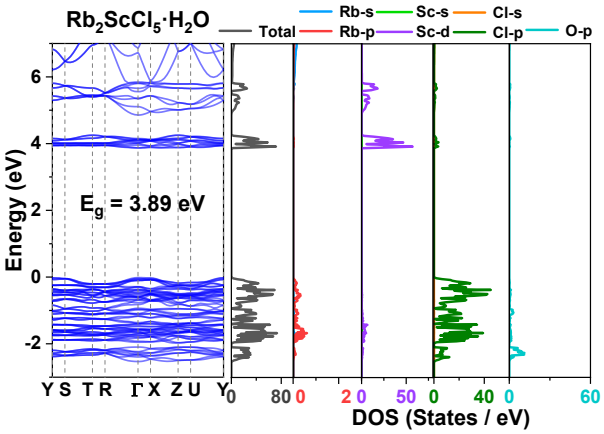

Fig. S13 Calculated electronic band structure (left) and DOS (right) of $Rb_2ScCl_5{\cdot}H_2O$ crystal.

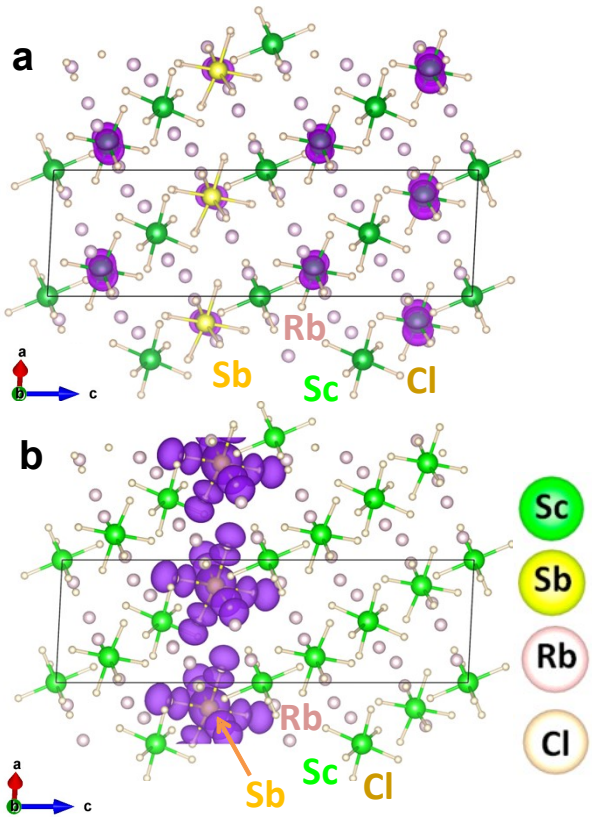

Fig. S14 (a) The conduction band minimum (CBM) and (b) the valence band maximum (VBM) associated charge densities of $Rb_3ScCl_6{:}Sb^{3+}$ crystal.

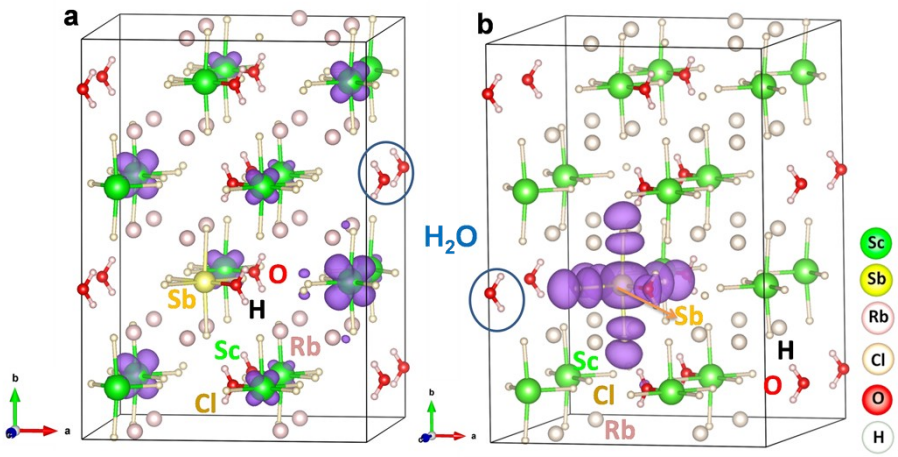

Fig. S15 (a) The conduction band minimum (CBM) and (b) the valence band maximum (VBM) associated charge densities of $Rb_2ScCl_5 \cdot H_2O:Sb^{3+}$ crystal.

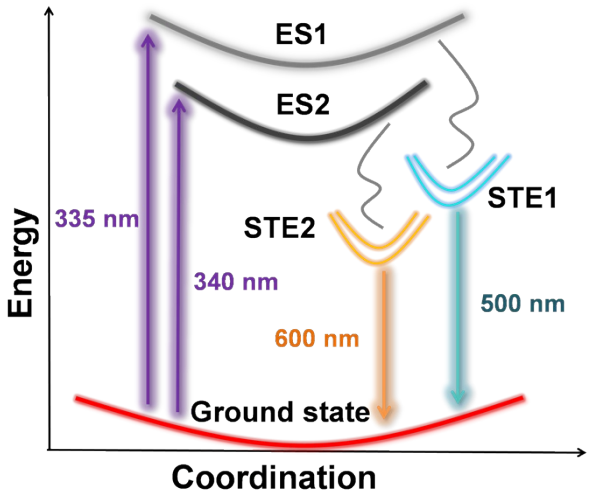

Fig. S16 Schematic illustration of the STE emission in Sb^{3+} doped $Rb_2ScCl_5 \cdot H_2O$ (600 nm) and Rb_3ScCl_6 (500 nm).

Table S1 Single crystal X-ray diffraction data of $Rb_2ScCl_5 \cdot H_2O$ single crystals.

Compound	$Rb_2ScCl_5 \cdot H_2O$
Formula weight	182.89g/mol
Temperature	298 K
Crystal system	Orthorhombic
Space group	*Pnma*
a/Å	14.003
b/Å	10.045
c/Å	7.246
α/°	90
β/°	90
γ/°	90
Volume/Å^3	1019.23
ρ_{cal}	2.979
F(000)	840
Limiting indices	$-16 \leq h \leq 15$
	$-11 \leq k \leq 10$
	$-8 \leq l \leq 8$
θ range/deg	2.91 to 25.00
Reflections collected	4199
Independent reflections	841[R(int) = 0.0303]
Absorption coefficient / mm^{-1}	0.0108
Data /restraints / parameters	951/3/56
Goodness-of-fit on F^2	1.041
Final R indices [I>2sigma(I)]	R1 = 0.0202
	wR2 = 0.0610
R indices (all data)	R1 = 0.0245
	wR2 = 0.0627

$R1=\sum(||F_o|-|F_c||)/\sum|F_o|$; $wR2=\{\sum[w(F_o^2-F_c^2)^2]/\sum[w(F_o^2)]^2\}^{1/2}$

Table S2 Comparison of Bond Length and Angles of $[ScCl_5H_2O]^{2-}$ in $Rb_2ScCl_5\cdot H_2O$ and $Cs_2ScCl_5\cdot H_2O$.[24]

	Bond Length(Å)		Angle (deg)	
$Rb_2ScCl_5\cdot H_2O$	Sc-Cl(1)	2.4873(15)	Cl-Sc-Cl	93.412(3)
	Sc-Cl(2)	2.4702(8)		
	Sc-Cl(3)	2.4702(9)		
	Sc-Cl(4)	2.4590(15)		
	Sc-Cl(5)	2.4510(14)		
	Sc-O	2.1710(3)	Cl-Sc-O	86.591(3)
$Cs_2ScCl_5\cdot H_2O$	Sc-Cl(1)	2.4822(8)	Cl-Sc-Cl	94.502(17)
	Sc-Cl(2)	2.4845(5)		
	Sc-Cl(3)	2.4845(5)		
	Sc-Cl(4)	2.4589(9)		
	Sc-Cl(5)	2.4593(8)		
	Sc-O	2.1793(3)	Cl-Sc-O	85.498(17)

Table S3 The decay of $Rb_2ScCl_5\cdot H_2O$:x%Sb^{3+} (x = 0.5, 1, 2, 3, 5, 8, 10, 15, 20).

Concentration (Sb^{3+}/mol%)	0.5	1	2	3	5	8	10	15	20
Decay (ns)	1.06	0.49	0.48	0.45	0.44	0.38	0.37	0.36	0.34

Table S4 Comparison of optical properties of Sb-doped $A_2BX_5 \cdot H_2O$ (A = Cs, Rb, B = In, Sc and X = Cl, Br) and A_3BX_6 (A = Cs, Rb, B = In, Sc and X = Cl, Br).

Perovskites	PLE (nm)	PL (nm)	PLQY (%)	FWHM (nm)	Year	Reference
$Cs_2InBr_5 \cdot H_2O$	355	695	33	/	2019	4
$Cs_2InCl_5 \cdot H_2O:Sb^{3+}$	/	560	90	/	2020	38
$Rb_2InCl_5 \cdot H_2O:Sb^{3+}$	/	600	90	/		
$Cs_3InCl_6:Sb^{3+}$	/	507	85	/		
$Rb_3InCl_6:Sb^{3+}$	/	497	95	/		
$Cs_2InCl_5 \cdot H_2O:Sb^{3+}$	344	610	73	164	2020	22
$Cs_2InBr_5 \cdot H_2O:Sb^{3+}$	357	692	33	207		
$Rb_2InCl_5 \cdot H_2O:Sb^{3+}$	310	678	51	211		
$Rb_2InBr_5 \cdot H_2O:Sb^{3+}$	395	766	18	160		
$Rb_3InCl_6:Sb^{3+}$	280	522	/	129	2020	5
$Cs_2InCl_5 \cdot H_2O:Sb^{3+}$	340	580	95	/	2020	12
$Cs_2InBr_5 \cdot H_2O:Sb^{3+}$	354	630	13	/		
$Cs_2InCl_5 \cdot H_2O:Sb^{3+}$	325	596	75	/	2022	13
$Cs3InCl_6:Sb^{3+}$	322	512	52	/		
$Cs_2ScCl_5 \cdot H_2O$	250	490	25	158	2022	24
	280	565	2	/		
	310	585	1	155		
$Cs_2ScCl_5 \cdot H_2O:Sb^{3+}$	310	585	≈100	/		
$Rb_2ScCl_5 \cdot H_2O$	/	/	/	/	This work	
$Rb_2ScCl_5 \cdot H_2O:Sb^{3+}$	340	600	99	141		
$Rb_3ScCl_6:Sb^{3+}$	340	500	96	102		